

# Mapping Topographic Structure in White Matter Pathways with Level Set Trees

Brian P. Kent<sup>1</sup>, Alessandro Rinaldo<sup>1</sup>, Fang-Cheng Yeh<sup>2</sup>, Timothy Verstynen<sup>3,\*</sup>

**1 Department of Statistics, Carnegie Mellon University, Pittsburgh, PA, USA**

**2 Department of Biomedical Engineering, Carnegie Mellon University, Pittsburgh, PA, USA**

**3 Department of Psychology and Center for the Neural Basis of Computation, Carnegie Mellon University, Pittsburgh, PA, USA**

**\* E-mail: timothyv@andrew.cmu.edu**

## Abstract

Fiber tractography on diffusion imaging data offers rich potential for describing white matter pathways in the human brain, but characterizing the spatial organization in these large and complex data sets remains a challenge. We show that level set trees—which provide a concise representation of the hierarchical mode structure of probability density functions—offer a statistically-principled framework for visualizing and analyzing topography in fiber streamlines. Using diffusion spectrum imaging data collected on neurologically healthy controls (N=30), we mapped white matter pathways from the cortex into the striatum using a deterministic tractography algorithm that estimates fiber bundles as dimensionless streamlines. Level set trees were used for interactive exploration of patterns in the endpoint distributions of the mapped fiber tracks and an efficient segmentation of the tracks that has empirical accuracy comparable to standard nonparametric clustering methods. We show that level set trees can also be generalized to model pseudo-density functions in order to analyze a broader array of data types, including entire fiber streamlines. Finally, resampling methods show the reliability of the level set tree as a descriptive measure of topographic structure, illustrating its potential as a statistical descriptor in brain imaging analysis. These results highlight the broad applicability of level set trees for visualizing and analyzing high-dimensional data like fiber tractography output.

## Introduction

Fiber tractography on diffusion weighted imaging (DWI) data can provide a high-resolution map of the anatomical connections between two brain areas [1]. The deterministic variant of fiber tractography generates a set of simulated fiber streamlines that provide rich information about the topographic structure of white matter pathways [2–4]. This method has been used recently to characterize the sheet-like layout of large, myelinated pathways [5], map the organization of fiber bundles within the same pathway [6–8], identify novel neuroanatomical patterns [9–12] and quantify the global structural connectivity between large sets of brain regions [3, 13], providing a so-called structural “connectome” of the human brain (see Van Essen et al. (2012) [14]). The topography and connectivity of the structural connections identified with fiber tractography have also been shown to relate directly to corresponding functional connectivity [15] and task-evoked functional dynamics [6, 16], highlighting the relationship between structure and function in neural systems. Despite these advances, the lack of descriptive metrics for the spatial topography of white matter pathways remains a standing problem with structural connectivity analysis (see Jbabdi et al. (2013) [17]).

Clustering is a popular method for summarizing the spatial structure in white matter tracks [18, 19], but clustering is often a difficult and ill-defined task. Many of the proposed approaches, such as fuzzy c-means [20, 21], spectral clustering [22, 23], diffusion maps [24], local linear embedding [25], geometric clustering [26, 27], and white matter atlas matching [28, 29], assume there is a single well-defined partition of the data into  $K$  separate groups, where  $K$  is presumed known *a priori*. However, when the data are

noisy or have a high degree of complexity or spatial heterogeneity, as is often the case in neuroimaging, it is more appropriate to assume the data have multi-scale clustering features that can be captured by a hierarchy of nested partitions of different sizes. These partitions and their hierarchy provide a wealth of information about the data beyond typical clustering results, unburdening the practitioner from the need to guess the “right” number of clusters, providing a global summary of the entire data set and offering the ability to select sub-clusters at different levels of spatial resolution depending on the scientific problem at hand.

There are many well-established hierarchical clustering methods, some of which have been applied to the problem of fiber track segmentation [30–33]. However, these methods often suffer from a lack of statistical justification. Single linkage clustering, for example, is known to be inconsistent in dimensions greater than one [34] and suffers from the problem of “chaining” [18]. The dendrograms that result from agglomerative hierarchical clustering do not indicate the optimal number of clusters; in order to obtain clusters the practitioner must specify the number of clusters or a threshold at which to cut the dendrogram. Furthermore, the dendrograms that result from these methods are rarely used as statistical descriptors in their own right.

Several recent fiber clustering analyses proposed more sophisticated methods that also do not require *a priori* knowledge of the number of clusters. Wasserman and Deriche (2008) [35] and Zvitia et al. (2008) [36] use the mean-shift clustering algorithm, which finds clusters that correspond to the modes of an assumed probability density function. Brun et al. (2004) use spectral clustering but avoid choosing a cluster number by doing recursive binary data partitions [37]. Wang et al. (2011) use a hierarchical Bayesian mixture model over supervoxels to estimate white matter segmentation, with the number of clusters chosen automatically by a Dirichlet process. Different clustering scales are achieved by defining supervoxels of various sizes [38]. Many of these methods are capable of clustering at multiple data resolutions, but this is typically not the focus and the multi-scale clustering results are typically not exploited for further analysis.

In this article we introduce and apply the principles of high-density clustering [39] for complex fiber tractography from a high-angular resolution form of DWI. We implement a general procedure called the *level set tree* for accurate estimation of nested subsets of high-density data points. Like other agglomerative clustering methods, the output of our procedure is a hierarchy of clusters that can be represented using a dendrogram. But unlike any other hierarchical clustering method, the dendrogram obtained by the level set tree procedure has a direct probabilistic interpretation in terms of underlying probability density function (see next section for details and background). As a result, level set trees provide a means to represent and visualize data arising from complex and high-dimensional distributions that is statistically accurate in the sense of being a faithful encoding of the level sets of a *bona fide* density function. This property extends to any sub-tree of a level set tree, so that with our procedure it is possible to extract subsets of data at multiple resolutions while retaining the same probabilistic faithfulness, effectively allowing for dynamic and multi-scale clustering that does not require advance knowledge of the true number of clusters.

In the context of fiber tractography, we show how the mode hierarchy of a level set tree can be used interactively to visualize spatial patterns and to cluster topographically similar fiber streamlines. Unlike most clustering methods that output a single partition of the data, level set trees encode many different cluster permutations and act as a scaffold for interactive exploration of clustering behavior. We also show how uncertainty can be captured on the level set tree, suggesting the potential for using the tree as a summary statistic of topographic structure. Taken together, our results demonstrate that level set trees offer a solution for describing the topographies found in fiber streamline data sets and provide a fundamentally new way of visualizing and analyzing complex spatial patterns in fiber tractography data sets.

## Methods

### Level set trees for densities

Suppose we observe a collection of points  $\mathbb{X}_n = \{x_1, \dots, x_n\}$  in  $\mathbb{R}^d$  and we want to identify and visualize the spatial organization of  $\mathbb{X}_n$  without specific knowledge about the data generating mechanism and in particular without any *a priori* information about the number of clusters. To be concrete, think of  $\mathbb{X}_n$  as the endpoints in  $\mathbb{R}^3$  of  $n$  fiber tracks, which we hope to describe in a way that is anatomically meaningful. Clustering is a common approach to this goal, but clustering is typically an ill-defined task because the concept of a cluster is vaguely defined. Our level set tree methodology, in contrast, extends the statistically principled approach to clustering in Hartigan (1975) [39].

Assume the data points are independent draws from an unknown probability distribution  $P$  on  $\mathbb{R}^d$  with probability density function (hereafter pdf)  $f$ . That is,  $f$  is a non-negative function such that the probability of observing a data point inside a subset  $A \subset \mathbb{R}^d$  can be computed as

$$P(A) = \int_{x \in A} f(x) dx, \quad (1)$$

where the integral is the Lebesgue integral in  $d$ -dimensions.<sup>1</sup> From this expression one can see that a set  $A$  where  $f$  takes on large values has a high probability of containing many of the sample points. As a result, points in the sample  $\mathbb{X}_n$  are likely clustered inside such a set, so it is natural to define clusters as regions of high density  $f$ .

To formalize this intuition, fix a threshold value  $\lambda \geq 0$  and let  $L_\lambda(f) = \{x \in \mathbb{R}^d : f(x) \geq \lambda\}$  be the upper level set of  $f$ , i.e. the set of points whose density values exceed the level  $\lambda$ . Call the set of connected components of  $L_\lambda(f)$  the  $\lambda$ -clusters of  $f$ . More generally, a high-density cluster of  $f$  is a  $\lambda$ -cluster for some  $\lambda$ ,  $0 \leq \lambda \leq \max_x f(x)$ . Notice that according to this probabilistic definition, the notion of a cluster depends on the choice of  $\lambda$  and that for a fixed  $\lambda$  the corresponding set of clusters will typically not give a partition of  $\{x : f(x) \geq 0\}$ . Also, for larger values of  $\lambda$  the  $\lambda$ -clusters define regions where the ratio of probability content to volume is higher.

A key feature of high-density clusters is the tree property: if  $A$  and  $B$  are two high-density clusters, then one is a subset of the other or they are disjoint. This implies that high-density clusters form a hierarchy—the *level set tree of  $f$* —that is indexed by the level values  $\lambda$ . The tree property is extremely advantageous for data analysis for a number of reasons. First, the level set tree can be depicted as a dendrogram, from which the overall hierarchy of clusters of  $f$  can be visualized across all possible levels of  $\lambda$ . In fact, one can regard the level  $\lambda$  as providing a clustering resolution of sorts, with lower values of  $\lambda$  corresponding to larger and coarser clusters and higher values to smaller, more sharply defined clusters. Thus, the dendrogram of level sets of  $f$  provides a multi-scale representation of the clustering characteristics of  $f$ . As a result, the practitioner is free to choose the scale and the number of clusters to extract, depending on the goals of the analysis. Contrast this with most popular clustering algorithms that implicitly adopt a single-scale approach and demand a choice of the number of clusters. Another advantage of the tree property is that it allows one to represent and store the entire set of cluster inclusions efficiently with a compact data structure that can be easily accessed and queried (see Table 5 and its description in the Results section. Finally, the dendrogram can be used in a direct and interactive manner for visualizing and extracting the clusters at various levels of the tree and for exploring the clustering features of a data set. With this approach, one can select a varying number of clusters at the same or different levels of  $\lambda$  without having to re-run the algorithm.

Figure 1 shows how to read and interpret the level set tree from a dendrogram. Panel A shows the pdf for a mixture of three Gaussian distributions and dashed lines representing four values of  $\lambda$ . For

<sup>1</sup>Technically,  $A$  must be a *measurable* subset of  $\mathbb{R}^d$  in order for the integral to be well defined. See Billingsley (2012) [40]. Throughout we will implicitly assume that measurability holds. From a practical standpoint, this is inconsequential.

each level the solid line segment depicts the corresponding clusters. Note that these are subsets of the real line, even though for illustrative purposes we depict them at the same level as the corresponding  $\lambda$ . The tree property can be seen in the fact that each high-density cluster is a subset of some cluster portrayed immediately below it but is disjoint from all other clusters at the same level. In panel B the dendrogram of the level set tree is shown; note how the hierarchy of clusters corresponding to the four levels is respected. Branching points correspond exactly to levels at which two or more modes of the pdf, i.e. new clusters, emerge. Each vertical line segment in this panel represents the high-density clusters within a single pdf mode. Line segments that do not branch are considered to be high-density modes, which we call the leaves of the tree. For simplicity, we tend to treat the terms *dendrogram* and *level set tree* as synonymous.

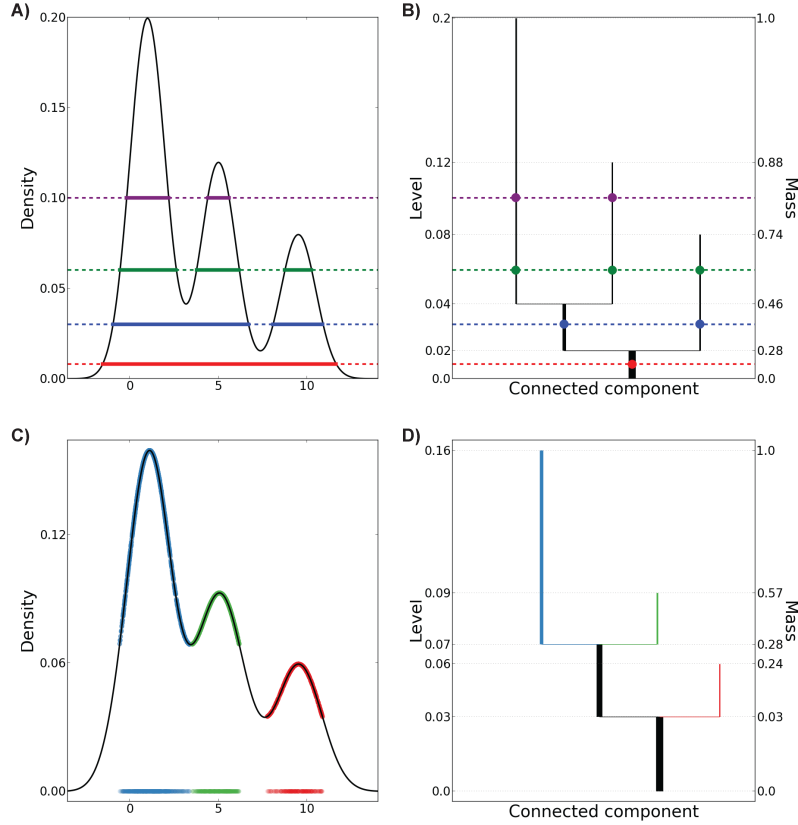


**Figure 1. Illustration of population and sample level set trees for a simple pdf.** A) The true pdf is a mixture of three Gaussians (black curve). For each of four example density levels (dotted lines), the high-density clusters are indicated by solid line segments. B) Population level set tree for the density in panel A. The high-density clusters of panel A are found at the intersections of the selected levels (dashed lines) with the tree. C) Estimated density (black curve) based on 2,000 data points sampled from the pdf in panel A. High-density points belonging to the leaves of the sample level set tree in panel D are shown on the horizontal axis and on the estimated density function. D) Level set tree estimate based on the sample in panel C. Leaves are colored to match corresponding points in the sample. For the purpose of illustration the trees in this figure are indexed by density levels, while all other trees in this article are plotted on the mass scale.



## Estimating level set trees

In practice  $f$  is not directly observed and one must use the data  $\mathbb{X}_n$  to compute an estimator  $\hat{f}$  of  $f$ . Under mild assumptions on  $f$  and if the sample size  $n$  is large,  $\hat{f}$  is guaranteed to be very close to  $f$  with large probability [41] and one could use the level set tree of  $\hat{f}$  to estimate the level set tree of  $f$  accurately. Unfortunately, computing the  $\lambda$ -clusters of  $\hat{f}$  is computationally infeasible even in small dimensions because finding the connected components of the upper level sets of  $\hat{f}$  requires evaluation of the function on a dense mesh in  $\mathbb{R}^d$  and a combinatorial search over all possible paths connecting any two points of such a mesh.

Instead, we propose a computationally tractable algorithm for level set clustering that combines and extends procedures outlined originally by Wishart (1969) [42] and more recently by Maier et al. (2009) [43], Chaudhuri and Dasgupta (2010) [44], and Kpotufe and von Luxburg (2011) [45]. At a high level, our algorithm approximates the level set tree of  $\hat{f}$  by intersecting the level sets of  $\hat{f}$  with  $\mathbb{X}_n$  and then evaluating the connectivity of each set by graph theoretic means. The details of the method are given in Tables 1, 2, 3 and 4. Our interactive Python toolbox for level set tree construction, analysis, and clustering is called *DEnsity-BASed CLustering (DeBaCl)* and is available at <https://github.com/CoAxLab/DeBaCl>.

**Table 1.** Conceptual level set tree estimation procedure

```

Inputs :  $\{x_1, \dots, x_n\}, k, \gamma$ 
Output :  $\hat{\mathcal{T}}$ , a hierarchy of subsets of  $\{x_1, \dots, x_n\}$ 
 $G \leftarrow \text{Compute.knn.graph}(\{x_1, \dots, x_n\}, k)$ 
for  $j \leftarrow 1$  to  $n$  :
     $\lambda_j \leftarrow \text{Compute.knn.density}(\{x_1, \dots, x_n\}, j, k)$ 
     $L_{\lambda_j} \leftarrow \{x_i : \hat{f}(x_i) \geq \lambda_j\}$ 
     $G_j \leftarrow$  subgraph of  $G$  induced by  $L_{\lambda_j}$ 
    Find the connected components of  $G_{\lambda_j}$ 
 $\hat{\mathcal{T}} \leftarrow$  dendrogram of connected components of graphs  $G_1, \dots, G_n$ , ordered by inclusions
 $\hat{\mathcal{T}} \leftarrow \text{Prune.tree}(\hat{\mathcal{T}}, \gamma)$ 
Return  $\hat{\mathcal{T}}$ 

```

The first step of our algorithm is to compute a k-nearest neighbor (knn) similarity graph  $G$  with nodes corresponding to  $\mathbb{X}_n$  and edges connecting vertex pairs if either node is one of the  $k$  closest neighbors to the other. In the second step, we compute a knn density estimator (Table 2) [43, 46], which we evaluate only at the  $n$  sample points. The parameter  $k$  controls the smoothness of the density  $\hat{f}$ ; larger values of  $k$  produce smoother and flatter density estimates with small variances but large biases. As a result, choosing a large  $k$  reduces the chance of finding spurious clusters but makes it harder to detect and separate true clusters that are very close to each other. Choosing a small  $k$  yields nearly unbiased density estimates with large variances. Based on our experiments and theoretical results ([47] and [48]), we tend to favor larger values of  $k$ .

Construction of the level set tree proceeds by ordering the estimated sample densities from smallest

**Table 2.** `Compute.knn.density`, a procedure for computing the k-nearest neighbor density estimate at the sample points.

**Inputs :**  $\{x_1, \dots, x_n\}, j, k$   
**Output :**  $\hat{f}(x_j)$  a knn density estimate for sample point  $x_j$   
 $r_k^d(x_j) \leftarrow$  k-nearest neighborhood of  $x_j$  among remaining sample points  
 $\hat{f}(x_j) \leftarrow \frac{k}{n \cdot v_d \cdot r_k^d(x_j)}$ , where  $v_d$  is the volume of the Euclidean unit ball in  $\mathbb{R}^d$   
**Return**  $\hat{f}(x_j)$

**Table 3.** `Compute.knn.graph`, a procedure for constructing a k-nearest neighbor similarity graph.

**Inputs :**  $\{x_1, \dots, x_n\}, k$   
**Output :** k-nearest-neighborhood graph  $G$   
**for**  $i \leftarrow 1$  **to**  $n$  :  
 $r_k^d(x_i) \leftarrow$  k-nearest neighborhood of  $x_i$  among the remaining sample points  
 $E \leftarrow \emptyset$   
**ForAll**  $i < j$  :  
**If**  $\|x_i - x_j\| \leq \max\{r_k^d(x_i), r_k^d(x_j)\}$  :  
 $E \leftarrow E \cup \{(i, j)\}$   
 $G \leftarrow (\{1, \dots, n\}, E)$   
**Return**  $G$

**Table 4.** `Prune.tree`. Removes small leaf nodes from a level set tree

**Inputs :**  $\hat{\mathcal{T}}$  (a hierarchy of subsets of  $\{x_1, \dots, x_n\}$ ),  $\gamma$   
**Output :** A pruned tree  $\hat{\mathcal{T}}$   
**For Each**  $A \in \hat{\mathcal{T}}$  :  
**If**  $|A| < \gamma n$  :  
 $\hat{\mathcal{T}} \leftarrow \hat{\mathcal{T}} \setminus A$   
**Return**  $\hat{\mathcal{T}}$

to largest and iterating over these values. For each value  $\lambda$  in this list, the upper level set is:

$$L_\lambda = \{x_i : \hat{f}(x_i) \geq \lambda\}. \quad (2)$$

In each iteration we construct an upper level similarity graph  $G_\lambda$  by removing the vertices from  $G$  whose sample points are not in  $L_\lambda$  and finding the connected components of  $G_\lambda$ .

The level set tree is the compilation of connected components over all values of  $\lambda$ . The final step is to prune small components of the tree that occur due to sampling variability or insufficient statistical power. Pruning merges components that contain fewer than  $\gamma n$  data points into other nearby components. Larger values of  $\gamma$  correspond to more aggressive pruning, where only connected components of large relative size are deemed as separate clusters. On the other hand, setting  $\gamma$  to be very small enhances the resolution of the clustering procedure but increases the chance of seeing spurious clusters.

### $\alpha$ -indexing

We have defined level set trees based on density thresholds, i.e. values of  $\lambda$ . Because this indexing is highly dependent on the height of  $f$  (or  $\hat{f}$ ), it lacks interpretability (for instance, it is not clear if  $\lambda = 1$  would be a threshold for high or low density regions). To remove the scale dependence, we instead consider indexing based on probability content rather than density height. Specifically, let  $\alpha$  be a number between 0 and 1 and define

$$\lambda_\alpha = \sup\{\lambda: \int_{x \in L_\lambda(f)} f(x) dx \geq \alpha\} \quad (3)$$

to be the value of  $\lambda$  for which the upper level set of  $f$  has probability content no smaller than  $\alpha$  [48]. The map  $\alpha \mapsto \lambda_\alpha$  gives a monotonically decreasing one-to-one correspondence between values of  $\alpha$  in  $[0, 1]$  and values of  $\lambda$  in  $[0, \max_x f(x)]$ . In particular,  $\lambda_1 = 0$  and  $\lambda_0 = \max_x f(x)$ . Because this map is monotonic, we can express the height of the tree in terms of the probability content  $\alpha$  instead of  $\lambda$  without changing the topology (i.e. number and ordering of the branches) of the tree. The  $\alpha$ -indexing is not, however, generally a linear re-indexing of  $\alpha$ , so the re-indexed tree will be a deformation of the original tree in which some branches are dilated and others are compressed. We refer to this probability-based scale as  $\alpha$ - or mass-indexing.

To estimate an  $\alpha$ -indexed tree, we index the level sets of  $\hat{f} \cap \mathbb{X}_n$  in a similar way. Specifically, for any  $\alpha \in \{0, \frac{1}{n}, \frac{2}{n}, \dots, \frac{n-1}{n}, 1\}$ , we set  $\lambda_\alpha$  to be the  $\alpha$ -quantile of the  $n$  estimated sample densities. The associated hierarchy of subsets  $L_{\lambda_\alpha}(\hat{f}) \cap \mathbb{X}_n$  is computed as  $\alpha$  varies from 1 to 0.

We regard  $\alpha$ -indexing as more interpretable and useful for several reasons. The  $\alpha$  level of the tree indexes clusters corresponding to the  $1 - \alpha$  fraction of “most clusterable” data points; in particular, smaller  $\alpha$  values yield more compact and well-separated clusters. The mass index can be used for de-noising and outlier removal: to eliminate 5% of the data with lowest estimated density, retrieve all the points in the clusters indexed by levels  $\alpha = 0.05$ . Scaling by probability content also enables comparisons of level set trees arising from data sets drawn from different pdfs, possibly in spaces of different dimensions. The  $\alpha$  index is more effective than the  $\lambda$  index for representing regions of large probability content but low density and is less affected by small fluctuations in density estimates.

### Pseudo-density analysis

A fiber track can be thought of as a set of points sampled along a random curve in three dimensions. Although probability distributions for these random functions are well-defined, they cannot be represented with pdfs [40]. We can extend level set trees to work with this type of non-Euclidean data by pseudo-density functions in place of pdfs [49]. Pseudo-densities cannot be used to compute probabilities as in Equation 1, but they can be regarded as measures of similarity among points and of the overall connectivity of a space.

To compute the sample level set tree for a collection of fiber tracks, we use the knn density estimate as in Table 2 but replace the Euclidean distance with a distance relevant to fibers, expunge the term  $v^d$  in the knn density calculation, and set  $d$  arbitrarily to 1. In general this does not yield a *bona fide* density

function, but it is sufficient to induce an ordering on the data points based on each point’s proximity to its neighbors.

We measure the proximity of a pair of fibers with with max-average-min distance [50], computed using the Dipy Python module’s `bundles_distances_mam` function [51]. Suppose a set of fiber tracks  $Z_1, \dots, Z_n$ , where  $Z_u$  is a sequence of  $r$  points  $\{Z_{ui}\}_{i=1}^r$ ,  $Z_{ui} \in \mathbb{R}^3$ . The distance between two fibers  $Z_u$  and  $Z_w$  is:

$$D(Z_u, Z_w) = \max \left\{ \text{mean}_i \{ \min_j d(Z_{ui}, Z_{wj}) \}, \text{mean}_j \{ \min_i d(Z_{ui}, Z_{wj}) \} \right\} \quad (4)$$

where  $d(Z_{ui}, Z_{wj})$  is the Euclidean distance between the  $i$ ’th point in fiber  $Z_u$  and the  $j$ ’th point of fiber  $Z_w$ . In practice, points with a small minimum distance to the other fiber are removed from the computation. Intuitively this distance matches each point in fiber  $Z_u$  to the closest point in fiber  $Z_w$  and *vice versa*, then averages the matched point distances that are sufficiently large.

Once the distance is computed for each pair of fibers, the pseudo-density function is evaluated for each fiber and a similarity graph is constructed. Level set tree construction then follows the procedure in Algorithm 1.

## Benchmark simulations

We compared the performance of level set trees in a traditional clustering task against several popular methods: k-means++ [52], gaussian mixtures [53], hierarchical agglomeration with the Ward criterion [39], hierarchical agglomeration with the single linkage criterion [53], spectral [54], diffusion map [55], and DBSCAN [56]. Each method was given the true number of clusters  $K$  in order to isolate the effectiveness of the algorithms from the heuristics for choosing  $K$ . For the sake of comparison we used the *fixed*  $K$  clustering option with level set trees, even though this ignores the ability of level set trees to automatically choose  $K$ .

Each method was tested in several three-dimensional data simulations with varying degrees of realism. The easiest simulation was a mixture of six Gaussian distributions, the moderate simulation was a mixture of three Gaussian distributions and three noisy arcs, and the difficult simulation was a resampling from a set of 10,000 striatal white matter fiber track endpoints for a real subject. For the latter scenario, the true clusters were determined by a careful application of level set tree clustering. To further vary the degree of difficulty of the clustering tasks, the group means in each scenario were contracted toward the grand mean by a coefficient  $r$ , which took 20 values on a grid ranging from 0.1 to 1.2. Finally, for each simulation type and separation coefficient, we drew 20 data sets of 5,000 points each. See Figures 5A, C, and E for examples of the simulation scenarios.

Both types of agglomerative hierarchical clustering were implemented with the R `hclust` function [57]. K-means++, Gaussian mixture modeling (GMM), and DBSCAN were implemented with the python module `scikit-learn` [58]. For DBSCAN we set the neighborhood parameter  $\epsilon$  to be the second percentile of all pairwise distances and the level set parameter (i.e. the number of neighbors required for a point to be a core point) to be the first percentile of pairwise distances. Note that DBSCAN does not allow  $K$  to be specified, making it difficult to compare to other methods.

We used our own implementations for spectral clustering and diffusion maps. For spectral clustering we constructed a symmetric knn graph on the data, with  $k$  set to one percent of the sample size. The points in the first percentile of degree in this graph were removed as outliers. For diffusion maps we used a complete similarity graph with Gaussian edge weights:

$$e(x_i, x_j) = \exp \left( - \frac{\|x_i - x_j\|^2}{\sigma} \right) \quad (5)$$

with  $\sigma$  set to twice the squared median of all pairwise distances [59]. For both spectral and diffusion map clustering we use the random walk form of normalized graph Laplacian:

$$L = D^{-1}(D - W) \quad (6)$$

where  $W$  is the similarity graph adjacency matrix, and  $D$  is the diagonal degree matrix for  $W$  [54]. For diffusion maps the  $i$ 'th eigenvector  $\psi_i$  is scaled by a function of its corresponding eigenvalue  $\rho_i$ :

$$\psi'_i = \left( \frac{1 - \rho_i}{\rho_i} \right) \psi_i \quad (7)$$

which creates a multi-scale diffusion map [60]. For spectral clustering and diffusion maps we use k-means++ to cluster the data after it is projected into the eigenspace, and for spectral clustering we use a knn classifier to assign outliers to clusters.

## Participants

Twenty male and ten female subjects were recruited from the local Pittsburgh community and the Army Research Laboratory in Aberdeen, Maryland. All subjects were neurologically healthy, with no history of either head trauma or neurological or psychiatric illness. Subject ages ranged from 21 to 45 years of age at the time of scanning and four were left handed (2 male, 2 female). All procedures were approved by the local institutional review board at Carnegie Mellon University.

## Imaging acquisition

All thirty participants were scanned on a Siemens Verio 3T system in the Scientific Imaging and Brain Research (SIBR) Center at Carnegie Mellon University using a 32-channel head coil. We collected a 50 min, 257-direction DSI scan using a twice-refocused spin-echo EPI sequence and multiple q values (TR = 9,916 ms, TE = 157 ms, voxel size =  $2.4 \times 2.4 \times 2.4$  mm, FoV =  $231 \times 231$  mm, b-max = 5,000 s/mm<sup>2</sup>, 51 slices). Head- movement was minimized during the image acquisition through padding and all subjects were confirmed to have minimal head movement during the scan prior to inclusion in the template. Since head motion cannot be reliably accounted for with a scan of this length, we opted instead to minimize head motion during acquisition.

## Diffusion MRI reconstruction

All DSI images were processed using a q-space diffeomorphic reconstruction method [61], implemented in DSI Studio (<http://dsi-studio.labsolver.org>). The coregistration was conducted using a non-linear spatial normalization approach [62], and a total of 16 iterations were used to obtain the spatial mapping function. From here orientation distribution functions (ODFs) were reconstructed to spatial resolution of  $2 \times 2 \times 2$  mm and a diffusion sampling length ratio of 1.25. To determine the average tractography space, we generated a template image (the CMU-30 Template) composed of the average whole-brain ODF maps across all 30 subjects.

## Fiber tractography

All fiber tracking was performed using DSI Studio. We used an ODF-streamlined region of interest (ROI) based approach [63] similar to that used in previous studies [7, 8]. Tracks were generated using an ODF-streamline version of the FACT algorithm [63–65]. For our initial test-set analysis, in MNI-space, we mapped two cortico-striatal pathways: lateral frontal (middle frontal gyrus to striatum) and orbitofrontal (gyrus rectus to striatum). For tractography analysis on the 30-subject template brain, a whole-brain seeding was used in the tractography process, with 300 seeds per voxel in the whole-brain mask (31,100,100 total). For the fiber endpoint analysis and the test-retest analysis, we only collected 10,000 streamlines per pathway per subject. This was done to minimize processing and computational demands in the level set tree generation process and to make equivalent comparisons across pathways with the same number of samples.

Fiber progression continued with a step size of 1 mm, minimum fiber length of 10 mm, and maximum of 70 mm. To smooth each track, the next directional estimate of each voxel was weighted by 20 percent of the previous moving direction and 80 percent by the incoming direction of the fiber. The tracking was terminated when the relative quantitative anisotropy (QA) for the incoming direction dropped below a preset threshold of 0.2 or exceeded a turning angle of  $75^\circ$ .

## Results

### Visualizing data with level set trees

Table 5 shows the raw information in an example level set tree. The tree is a collection of nodes; each node has start and end  $\lambda$  and  $\alpha$  levels, a parent, children (possibly an empty set), and constituent data points at the node's start level. This information is conveyed more effectively through a plot of the dendrogram. Figure 1C illustrates a density estimate for 2,000 points sampled from a mixture of three Gaussian distributions and Figure 1D shows the estimated level set tree for the sample. Each vertical line segment of the tree represents the clusters contained in one mode of the estimated pdf; all of these clusters are subsets of the cluster at the start level of the mode.

**Table 5. Estimated level set tree information for a simple data simulation.**

Node	Start Level	End Level	Start Mass	End Mass	Size	Parent	Children
0	0.000	0.005	0.000	0.021	2001	None	[1, 2]
1	0.005	0.061	0.021	0.528	1309	0	[3, 4]
2	0.005	0.165	0.021	0.998	649	0	$\emptyset$
3	0.061	0.167	0.528	0.999	359	1	$\emptyset$
4	0.061	0.172	0.528	0.999	295	1	$\emptyset$

The tree visualization contains several other pieces of information. The height of each tree node indicates the prominence of the corresponding density mode. Nodes are sorted so that density modes containing more sample points (i.e. mass) appear to the left of smaller siblings. The mass of each node is also proportional to the thickness of its line segment and the amount of whitespace surrounding its line segment. For example, in Figure 1D, the first split yields two nodes containing approximately 75% (black node) and 25% (red node) of the mass respectively, so the black segment is thicker and surrounded by whitespace occupying about 75% of the width of the plot.

The mode hierarchy shown in a level set tree is a natural platform for interactively exploring interesting subsets of complicated data; by selecting a tree branch one can zoom in on structurally coherent groups, ameliorating overplotting problems to a great extent. Figures 2 and 3 illustrate the use of level set trees for interactive data visualization on a set of end point locations from 10,000 streamlines tracked from the lateral frontal cortex to the striatum. Figure 2B shows each streamline endpoint, color coded by its local density (higher densities are shown in warmer colors). The tree for this data set (Figure 2C) is more complicated than the tree in Figure 1. It shows there are two primary clusters, each of which is further separated into well-defined sub-groups.

In Figure 3 we use the tree to navigate through this data set. Selecting the data points associated with one of the large primary branches (Figure 3A and 3B) shows that this high density region is spatially isolated in a single cluster in the dorsal portion of the striatum, specifically the dorsal culate nucleus. By zooming in on some of the smaller components of the other primary branch (Figure 3C and 3D) we see that these are reflected as independent sub-clusters from the first branch, with endpoints in the anterior aspect of the caudate near the shell region of the nucleus, with local density hierarchies within

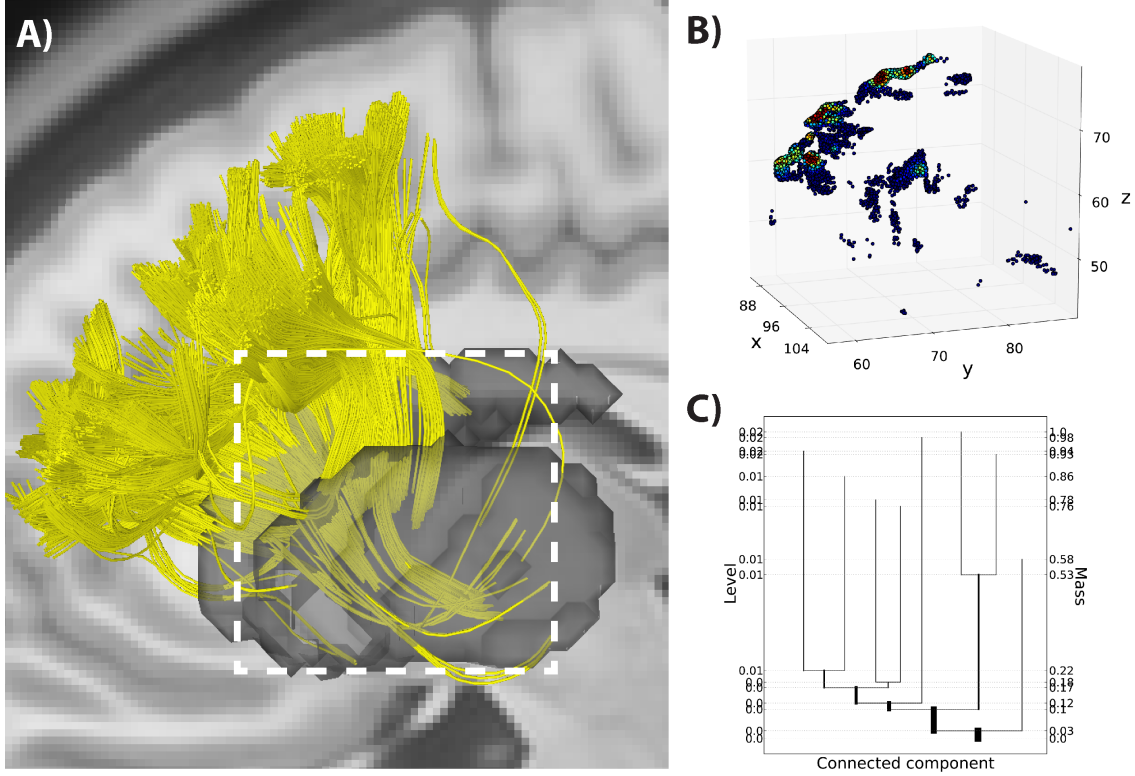


**Figure 2. Level set tree for cortico-striatal fiber endpoint locations.** A) 10,000 streamlines (yellow) mapped from the lateral frontal cortex (middle frontal gyrus) to the striatal nuclei (caudate nucleus, putamen and nucleus accumbens) shown as a gray region of interest (ROI). Data taken from a representative subject. B) Endpoint locations (in millimeters) of the streamlines shown in panel A, colored by estimated density (red is high). C) The corresponding level set tree, which indicates a complex cluster structure in these data. A major split occurs when 10% of the data are excluded from the density upper level set, and each branch of the split has relevant sub-clusters at various resolutions. Note the lack of information in the density level index on this plot, which is a typical outcome.

the cluster (Figure 3D). This illustrates how, by interacting with the different branches of the level set tree, it is possible to characterize local topographic structures at different resolutions that reflect known, anatomically distinct sub-regions of the projections into the caudate [66].

### Clustering with level set trees

Level set trees have several useful properties for solving practical clustering problems. Most notably, they provide several different ways to obtain cluster labels, some of which do not require *a priori* knowledge of the number of clusters. They also remove outliers automatically and allow an investigator to visualize many different clustering permutations simultaneously and interactively. Figure 4 shows the output from three of the tree-based cluster labeling methods applied to the same endpoint distribution shown in Figures 2 and 3 (see Methods).

By construction, the tree is a compilation of connected components over the levels of a pdf estimate, so the most straightforward way to cluster is to retrieve the connected components at a chosen density

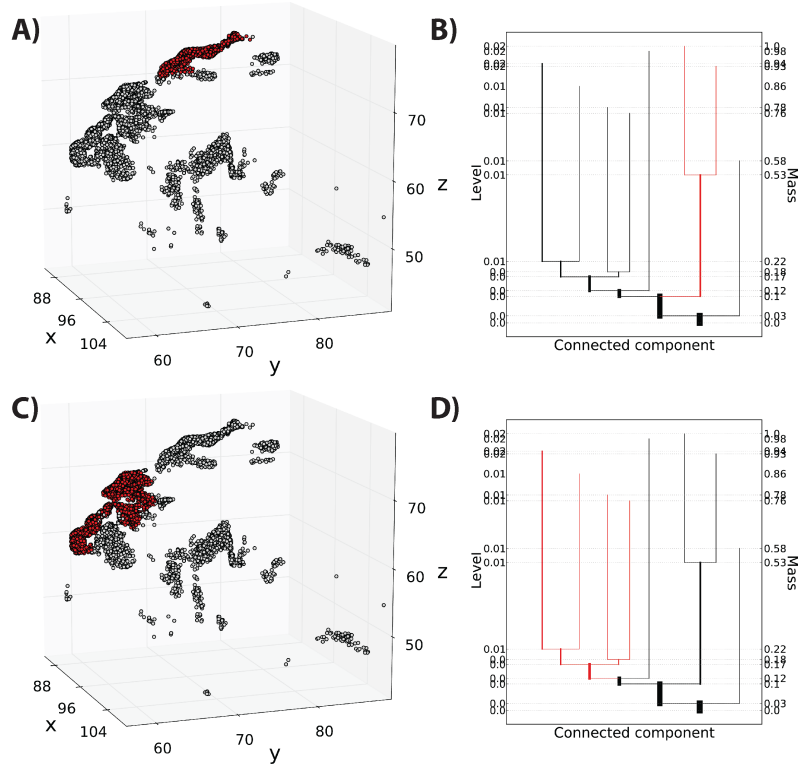


**Figure 3. Exploring data subsets with a level set tree.** A) Striatal endpoints from Figure 2. Red points are members of a selected node of the level set tree, shown in red in panel B. C) Striatal endpoints belonging to a different mode of the level set tree, shown in panel D.

or mass level (Figures 4A and 4B). In addition to its definitional nature, this method conveys the most intuitive sense for where the highest density data subsets are located. It also allows the investigator to control the number of points in the clusters; choosing a low mass level produces clusters that contain most of the data, while high mass thresholds produce clusters with only the peaks of the data modes. Finally, this method avoids the need to specify *a priori* the number of clusters, which must be chosen heuristically in many popular clustering methods (k-means, for example).

The drawback of clustering at a single level is that it requires an arbitrary choice of  $\lambda$  or  $\alpha$ . All-mode clustering, which uses each leaf node of a level set tree as a cluster, also automatically chooses the number of clusters and avoids the arbitrary choice of a density or mass level at which to cut the tree [67] (Figures 4C and 4D). This method does remain sensitive to the choice of smoothing and pruning parameters, however. For a given degree of pruning, this method tends to produce more and smaller clusters than level set clustering.

If the clustering task demands a pre-set number of clusters,  $K$ , this can be done with a level set tree by identifying the first  $K$  disjoint components to appear in the tree as the level increases from  $\lambda = 0$ . Unlike k-means (and related methods), there is no guarantee that there will be  $K$  disjoint nodes in a level set tree (Figures 4E and 4F).

In general, each method of labeling can capture general streamline clusters approximately near macroscopic divisions of the striatal nuclei. For instance, the red branch in each panel of Figure 4 highlights an isolated cluster of prefrontal projections that terminate on the putamen. The remaining clusters on



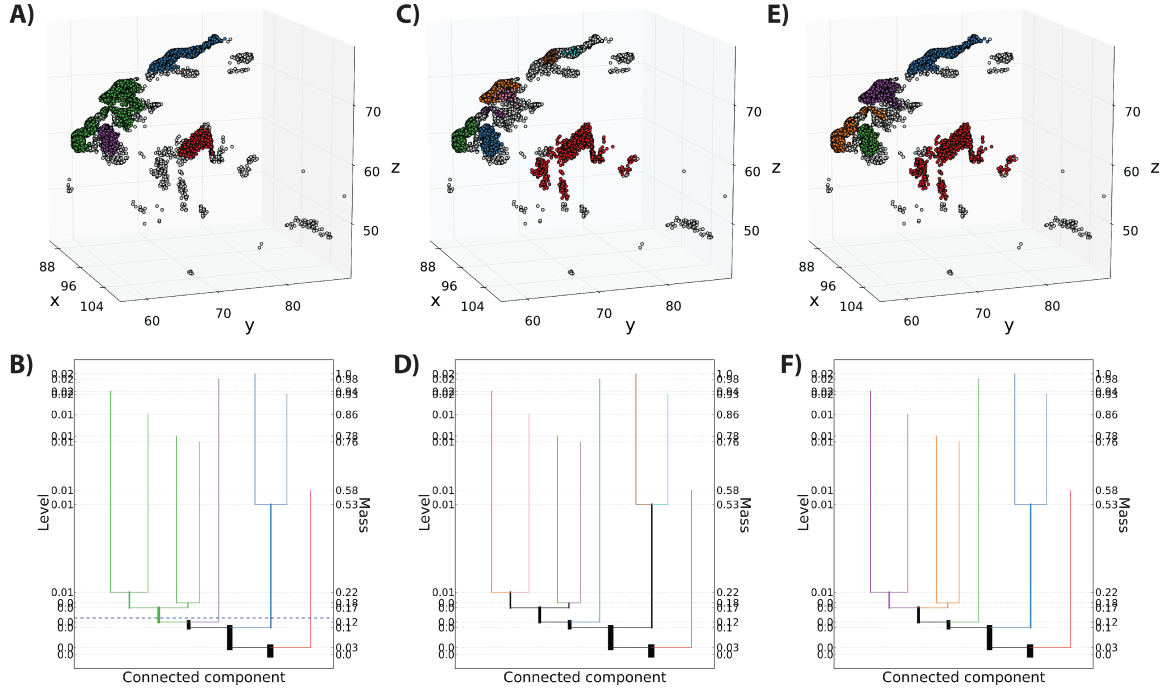


**Figure 4. Clustering with a level set tree.** A, C, E) Striatal endpoints colored by cluster assignment for three different cluster labeling methods. Gray points are unassigned because their estimated density is too low. Cluster colors match the tree node colors in the panels below. B) Tree nodes corresponding to clusters in panel A. These nodes are selected by cutting across the tree at a desired density or mass level. This method is very straightforward because it is based on the definition of the tree. D) Tree nodes corresponding to clusters in panel C. Each leaf of the tree produces a cluster. F) Tree nodes corresponding to clusters in panel E. The tree is traversed upward from the root (or roots) until the desired number of clusters first appears.

the caudate nucleus also break down into two major sets of endpoints. One set (dark blue in Figures 4A and 4E, brown and cyan in Figure 4C) identifies clusters of streamlines that terminate on the tail of the caudate, while the third major set (green and purple in Figure 4A; orange, green and blue in Figure 4C; orange, green and purple in Figure 4E) identifies streamlines terminating about the shell of the caudate nucleus. Thus, the first three branches of the level set tree appear to capture known anatomical subdivisions of inputs to the striatum, with slight differences in sub-cluster identification depending on the labeling approach used.

Each of these three methods typically assigns cluster labels to a fraction of the sample, which we call the foreground points. The by-product of this is the intelligent removal of outliers. Figure 4 shows that the size of the foreground and outlier sets can vary greatly depending on the choice of clustering method and parameter values. In particular, the all-modes technique tends to create a large number of small clusters. When a full segmentation is needed, the unlabeled background points can be assigned to a cluster with any classification technique.

Together, the advantages of a level set tree approach—avoiding the need to specify the cluster number, multiple clustering methods, visualization of many cluster permutations, interactive clustering exploration, and automatic outlier removal—allow the practitioner to gain greater insight into the clustering behavior of a data set, using fewer assumptions than would be necessary for standard methods.

## Clustering performance evaluation

To analyze the effectiveness of level set tree clustering we tested it in a range of simulations against several standard clustering methods: k-means++, gaussian mixture models, hierarchical agglomeration, spectral clustering, diffusion map clustering, and DBSCAN. The simulations ranged in difficulty over both the degree of separation of the clusters and the type of data generating process, with the most complex scenario closely mimicking fiber track endpoint distributions (see Methods for more detail).

Not surprisingly, for the easiest clustering task—a mixture of six spherical Gaussian distributions—all methods achieved perfect identification of the true clusters when the groups were well separated. Single linkage hierarchical clustering had a very high error rate even at medium degrees of separation between clusters, due to the well-studied problem of chaining. The density-based methods DBSCAN and level set trees also required more separation between clusters before achieving the same error rate as parametric methods, possibly due to the challenge of assigning low-density points to a cluster.

The results are more difficult to interpret for the moderately difficult simulation scenario with three arcs and three spherical Gaussians. Single linkage hierarchical clustering again required the most separation between clusters to achieve highly accurate classification. Spectral clustering was perfect when the clusters were well-separated and was as good as any other method when the clusters were very close, but performed poorly at mid-range degrees of separation. The closely related technique of diffusion maps actually became less accurate at large degrees of separation. Level set tree clustering performed poorly for tightly packed clusters, but was comparable to the parametric methods (K-means++, Ward linkage, and GMM) for somewhat and very well separated clusters.

While the second simulation type is more challenging than the mixture of only Gaussians, it remains much simpler than the highly non-convex, multi-resolution data in many fiber tractography clustering tasks. To test the clustering methods in a more realistic setting we generated simulated data sets by randomly resampling 5,000 points from a set of 10,000 striatal white matter fiber track endpoints from one subject and adding Gaussian noise to each resampled point. True group labels were assigned with a careful application of level set clustering, and as with the the easy and moderate scenarios, we modulated the difficulty of the task by contracting the clusters toward the grand mean to varying degrees.

In this much more complicated and realistic setting, the parametric methods performed poorly, achieving only about 70% accuracy, even when the clusters are very well separated. Each of the nonparametric methods (level set clustering, DBSCAN, diffusion maps, and spectral clustering) performed best at some degree of separation, making it difficult to identify clearly superior or inferior methods. DBSCAN and level set trees have accuracies somewhat less than 100% even for well-separated clusters, probably due to the problem of assigning low-density points to clusters. A more nuanced classifier for this step in level set tree clustering would likely improve the results for level set trees in particular.

Level set trees enjoy several categorical advantages over methods like spectral clustering and diffusion maps, namely a more intuitive representation of data structure, facilitation of interactive data exploration, a concise representation of many different clustering permutations, and automatic selection of the number of clusters. This experiment suggests level set trees are also at least as accurate in practical clustering tasks, particularly with challenging nonconvex clusters.

Finally, we take note that we have made no attempt to choose the parameter  $k$  in an optimal manner in our experiments.

## Whole fiber segmentation

So far our analysis has focused on level set trees that are generated using just the 3-dimensional endpoint locations of the fiber streamlines that terminate in the striatum. This ignores the rich data contained in the rest of each fiber streamline, which can provide substantially more information about differences between sets of fibers than just the location of the streamline ends. We adopted a pseudo-density approach for whole-fiber level set trees, where a pairwise fiber distance is used to rank each streamline according

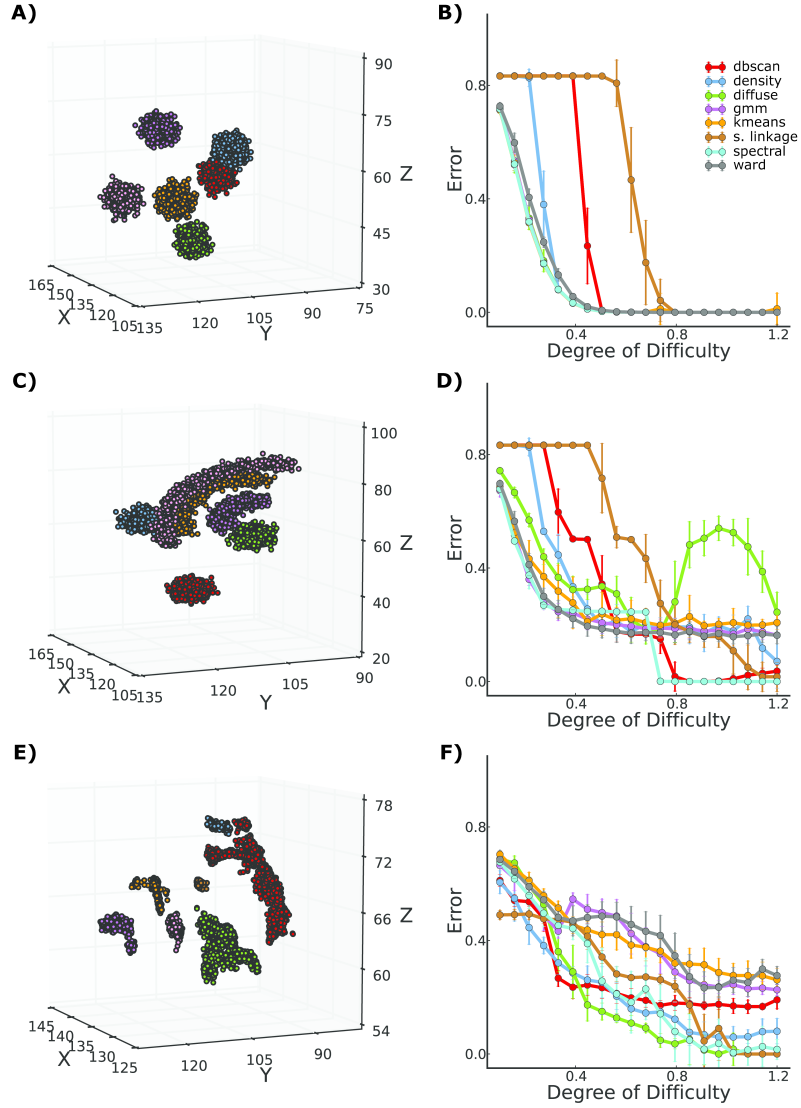


**Figure 5. Comparison of clustering method accuracy in simulations.** A, C, E) Example draws from each of three simulation scenarios (Gaussians, arcs & Gaussians, and resampled striatal endpoints, from the top), with observations colored by true group label. B, D, E) Error rate for each type of simulation. For each simulation, the degree of clustering difficulty was varied by contracting the groups toward the grand mean by various amounts, so that most methods are accurate when the groups are well-separated and inaccurate when the groups overlap. For each type of simulation and each degree of difficulty, the mean and standard deviation of classification error are reported for 8 clustering methods: DBSCAN (dbscan), level set tree clustering (density), diffusion maps (diffuse), Gaussian mixture models (gmm), k-means++ (kmeans), hierarchical clustering with single linkage (s.link), spectral clustering (spectral), and hierarchical clustering with linkage by the Ward criterion (ward).

to the spatial proximity of its neighbors (see Methods). This pseudo-density ranking is not a true pdf because it is not normalized to sum to one, but it can be used just like a density function to define and

index upper level sets. We use the max-average-min fiber distance, which matches each point on a fiber to the closest point on a second fiber, then averages these distance and finds the maximum of the averages over the fiber pair (see Methods). In this way the level set tree uses non-Euclidean distance as a factor in the whole-fiber clustering process.

We used the pseudo-density level set tree approach to look at the organization of cortico-striatal projections from two areas, the lateral frontal cortex and orbitofrontal cortex, in the 30 subject template brain (Figure 6). In the lateral frontal cortex we detected seven clusters of streamlines (34,982 foreground fibers out of 51,126 total fibers) that were organized in a consistent, evenly spaced rostral-caudal direction along the middle frontal gyrus (Figure 6A), an organization that is consistent with previous reports in both the animal and human literatures [8,66,68]. Each identified cluster reflects regions of high pseudo-density along the middle frontal gyrus. It is important to note that this whole-fiber clustering was able to capture divergent patterns in the white matter pathways. The dark blue and cyan streamlines start in the same region of the middle frontal gyrus, but diverge to different sub-cortical targets (namely, the caudate and putamen). This split is easy to identify in the level set tree by the emergence of an early branching in the tree into two major divisions that reflect caudate versus putamen fibers (Figure 5B). This provides a clean anatomical segmentation of the fibers despite the fact that these two fiber sets start in the same region of the middle frontal gyrus.

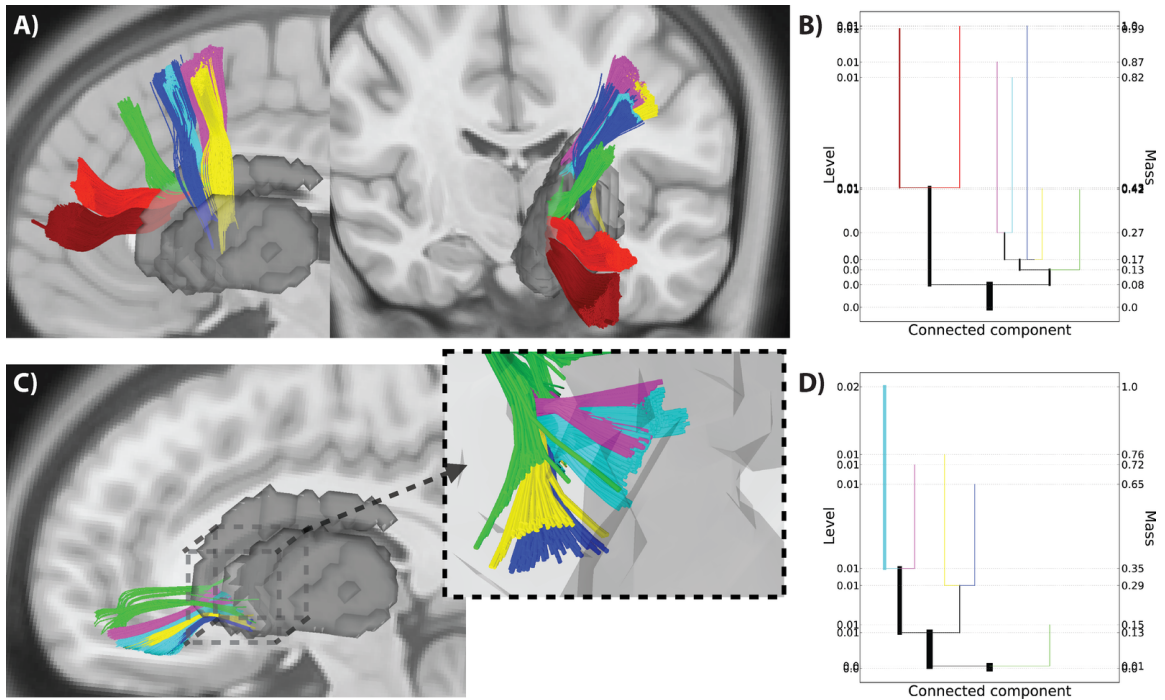


**Figure 6. Level set tree clustering for whole fiber streamlines.** A) Foreground fibers for the seven selected clusters from the 30 subject template data set for streamlines tracked between the middle frontal gyrus and striatum, shown in both a sagittal and coronal view. Clusters are colored according to an all-mode clustering of the tree. B) The level set tree for data in panel A. Tree leaves are matched to fiber clusters by color. C) Same analysis as shown in A, but for a set of streamlines from the orbitofrontal cortex. Inset shows closeup of fiber streamlines in the striatal ROI mask. D) Level set tree for data shown in panel C. The branch colors of trees in panels B and D match the clusters shown in the streamlines of panels A and C respectively.

In the projections from the orbitofrontal cortex we identified five mode clusters (Figures 6C and 6D). Close inspection of the endpoints of these streamlines in the striatum reveals that each cluster forms a striated-like pattern in the caudate that is similar to patterns previously reported in corticostriatal projections [8] (Figure 6C, inset). These striated formations are thought to reflect the modularized biochemical makeup of the striatum [69, 70]. This complex arrangement is difficult to capture with clustering methods that assume convex cluster shapes, but the whole-fiber pseudo-density clustering approach successfully extracts the patterns with minimal assumptions.

## Level set tree variability

To assess the stability of the 30 subject template level set trees in Figure 6, we created a set of trees by subsampling from the original lateral and orbitofrontal fiber streamline data sets and constructing a tree for each subsample. This simulates the variability seen when repeating the tractography on the same data set multiple times. The overlaid tree plots in Figures 7A and 7D indicate a high degree of stability for the trees built from these subsampled data sets, although it appears that the stability might be slightly lower for the orbitofrontal set. This conclusion is supported for both ROIs by the mode function overlays and histograms of mass values where each tree splits. These plots illustrate that the existence of each tree branch is consistent across the subsamples, even though there is some variation in the mass levels where the branches first appear.

The high degree of stability in these subsample trees conveys certainty to the features of the level set trees constructed on the full data set (Figures 6B and 6D). For example, the left branch of the tree for the lateral frontal projections contains two prominent nodes (red and dark red) that appear when 42 percent of the fibers are in the background (i.e. not in the the upper level set). The fact that this same split occurs in every one of the subsample trees is evidence that such a split exists in true underlying (and unobserved) distribution of fibers that generated this data set.

On the other hand, data sets that differ even in seemingly small ways can lead to much more variation in the resulting level set trees. For a subset of subjects, fiber streamlines were reconstructed for two separate scans separated by six months. Figure 8 shows the level set trees constructed for the lateral frontal projections from each scan in several example subjects, as well as the foreground clusters produced by all-mode clustering. The foreground clusters reveal that there does tend to be an overall high degree of similarity between the fiber streamline sets across trials, with the exception of one or two well-defined clusters that only appear in one of the two scans (highlighted in gray in Figure 8).

The level set trees likewise reflect similar structure across scans, but the non-overlapping tree nodes appear to exaggerate the differences between trees. For example, panels E and F in Figure 8 show the foreground fiber streamlines and level set trees for two scans of a single subject. The blue, green, cyan, violet, and yellow clusters match well across scans and appear to share very similar topography. However, panel E contains an obvious cluster on the right side of the plot (in gray) that is not present in panel F, while panel F contains its own obvious cluster on the left side of the plot (also in gray) that is not present in panel E. Note that each branch's (or cluster's) color was manually defined to match between images of the same subject, but does not necessarily reflect the same branch/cluster identified across subjects. While some of the features of the trees reflect the overall similarity—for example, the number of leaves is the same and the yellow, cyan, and violet clusters are more similar to each other while the blue cluster is much different—the overall shape of the trees is very different.

These variations reflect actual differences between the test and retest data, not just variability of the level set tree procedure. Not only are some clusters present in only one of the two data sets (shown in gray in Figure 8), but differing tree shapes and branching locations indicate that the probability content and relative hierarchy of even similar-looking clusters is not the same across scans. Despite such marked differences in the test and retest data sets, the output from all-mode clustering retains a very high degree of consistency across scan sessions, demonstrating the robustness of the proposed methodology.

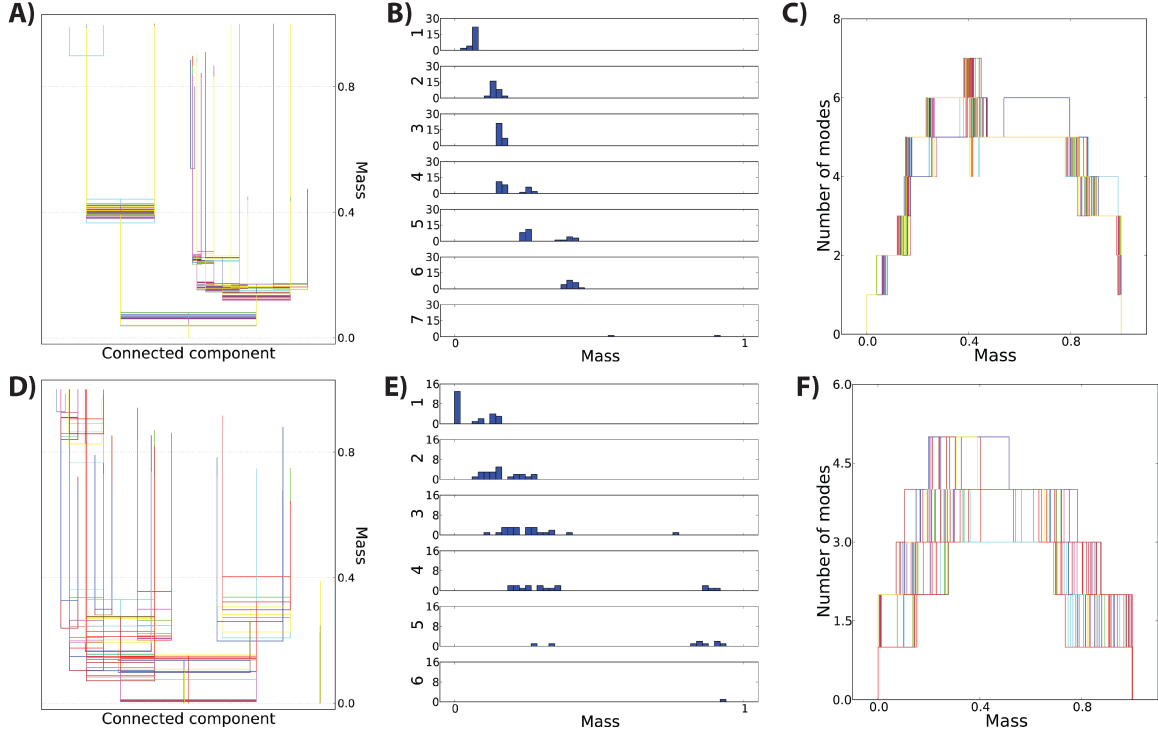


**Figure 7. Repeat reliability for level set tree results for a 30-subject template, using subsampling.** For the middle frontal gyrus ROI, 28 random subsamples of 15,000 fibers were drawn from the total of 51,126 fibers, while 1,500 fibers were drawn for 23 subsamples from the 3,038 total fibers in the rectus. A) All 28 level set trees plotted on the same canvas, illustrating the high degree of similarity between the data structure in the subsamples. B) Histograms of the mass levels of the splits over the whole set of subsample trees. Split mass levels are matched across subsamples by rank order. C) All 28 mode functions plotted together, illustrating that there is little variation in the number of clusters at each mass level. D) All 23 level set trees plotted together. E) Distribution of mass values for splits, matched across subsamples by rank within each sample's tree. F) All 23 mode functions overlaid.

## Discussion

White matter pathways have highly complex shapes and spatial organization, making it difficult to summarize their topographic structure. We have shown that level set trees provide a concise representation of this topography by describing the hierarchy of modal regions in the density or pseudo-density function that describes the probabilistic spatial distribution of a set of fiber tracks. We demonstrated that this hierarchy is useful by identifying not only major anatomical boundaries in the striatum (e.g., putamen vs. caudate), but also sub-regions within the same nucleus (e.g., shell vs. tail of the caudate; see Figure 4). We demonstrated the reliability of these results through qualitative comparisons of level set trees in repeated sub-sampling and test-retest experiments, suggesting that level set trees have the potential be used as statistical estimators of fiber streamline topography. Finally, we evaluated the performance of level set trees in several simulations against a suite of standard clustering methods that are commonly used to describe fiber streamline organizational patterns. Level set trees performed as well as any of the clustering methods, however we should also emphasize that describing fiber track topography and

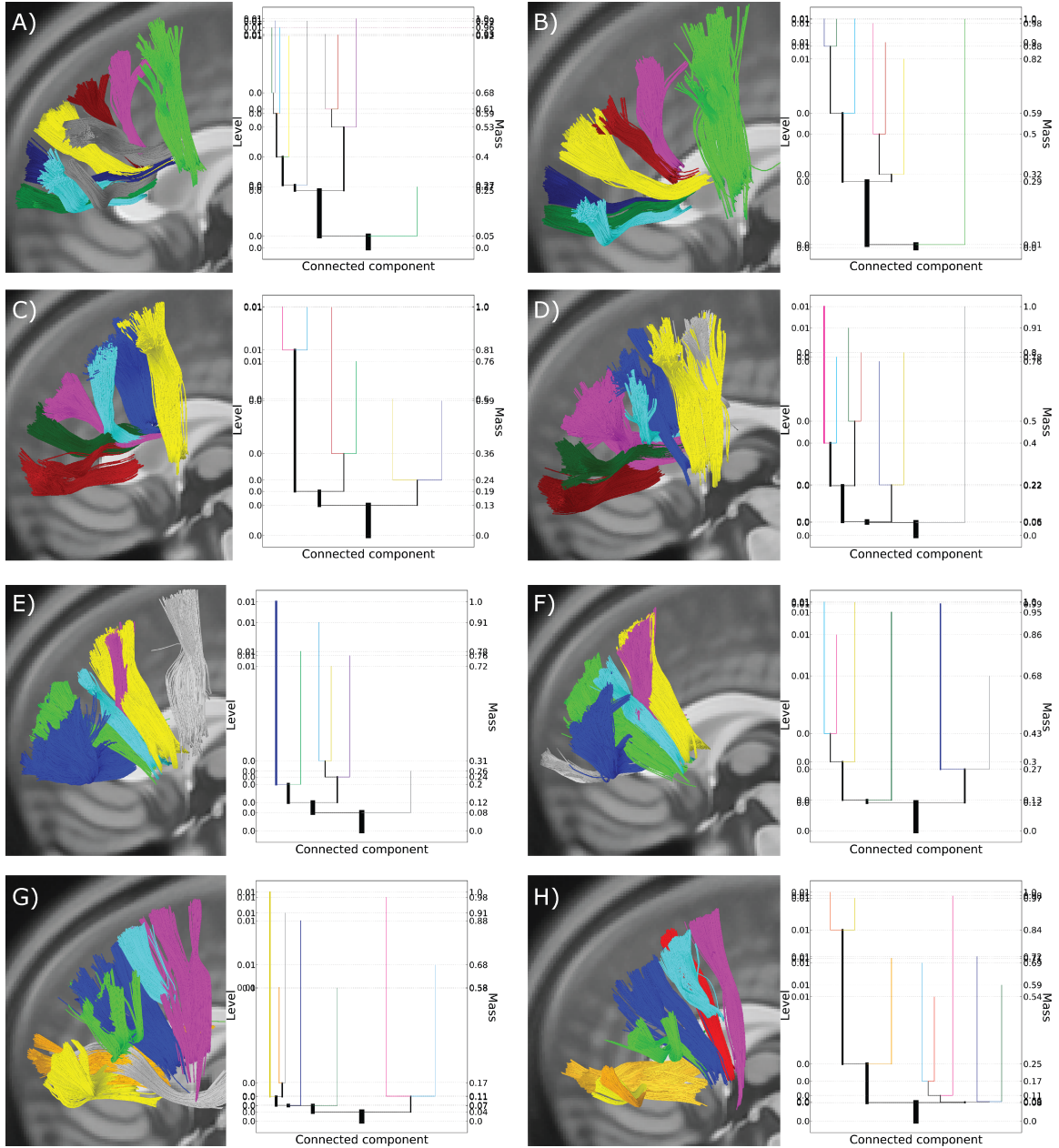


**Figure 8. Test-retest comparisons for four subjects, tested six months apart.** Colored streamlines show clusters that were consistently observed at both scan times. Gray streamlines show clusters detected at only one time point. Panels A, C, E, and G show results from the initial scan session. Panels B, D, F, and H show results from the second scanning session six months later.

clustering these data points are not equivalent tasks. For the purpose of summarizing topography, level set trees have several advantages over traditional clustering techniques: they are statistically principled; they are compact data structures that enable fast retrieval of high-density clusters at any density level;



they allow a multi-scale visualization of the cluster patterns in a data set; they are a natural platform for interactive data exploration; and they offer several methods for obtaining particular cluster labels without assuming the number of clusters and with automatic removal of outliers.

Level set trees are traditionally based on an estimate of an unobserved pdf that is assumed to have generated a data set, which is a realistic assumption for fiber streamline endpoints. We show for this type of data how level set trees can be used to visualize data patterns, interactively explore structurally coherent data subsets, and simultaneously present many different cluster labelings. Where the assumption of a pdf is not realistic, as with infinite-dimensional whole fibers, we extend level set trees to address the problem of describing the topography by observing that a pseudo-density estimator (along with a similarity measure) is sufficient for level set tree construction.

Ideally, level set trees could be used as statistical tool for inference when comparing white matter topographies across populations. For example, does the organization of fiber streamlines between two brain areas differ in individuals with neurological disorders (e.g., autism) when compared to neurologically healthy controls? By qualitatively demonstrating the reliability of level set tree structure, we highlight this potential of the method. Quantification of the uncertainty in level set trees is an open research problem; the qualitative comparisons shown in this paper as well as other preliminary work in this direction [48,71,72] have shown that level set trees constructed on data drawn from the same distribution tend to be very similar, or stable, while trees constructed on data drawn from different distributions tend to be different. Stability is a difficult principle to apply, however, because simply identifying when two trees are similar is also an open research area (one that deserves future attention, but is well beyond the scope of the current project).

An important limitation of our methodology is the selection of tuning parameters  $k$  for connectivity and density (or pseudo-density) estimation and  $\gamma$  for tree pruning (although the choice of cluster number is not required as with most clustering methods). We could choose these parameters based on the optimal values found in the theoretical literature [41] but these values are only valid in asymptotic regimes (where the sample size increases) and tend to work poorly in practice. As a result, as with much of applied statistics, selecting tuning parameters requires sound empirical judgment. It should be noted, however, that in our experiments the results tend to be robust for a relatively large range of tuning parameter values. Because there are several ways to obtain clusters from level set trees, inserting level set tree methods into an automated data analysis pipeline also requires a choice of cluster labeling method, in addition to the tuning parameters.

Despite these limitations, level set trees are a novel and powerful way to analyze the topography of fiber streamline data sets with minimal *a priori* assumptions. As DWI methodologies improve, the usefulness of this approach for characterizing sub-divisions in anatomical pathways will allow for greater specificity of regions of interest. Originally intended to describe probability density functions, level set trees can be extended to model pseudo-density functions as well, allowing us to apply the trees' powerful data visualization and clustering tools to the analysis of fiber streamline data sets. This flexibility opens the potential for this method of density-based clustering approaches to be used in a variety of neuroimaging analyses beyond white matter tractography. Future work will focus on these extended applications in a neuroimaging context.

## References

1. Hagmann P, Jonasson L, Maeder P, Thiran Jp, Wedeen VJ, et al. (2006) Understanding Diffusion MR Imaging Techniques : From Scalar Diffusion-weighted Imaging to Diffusion Tensor Imaging and Beyond. *Radiographics* 26: 205–224.
2. Descoteaux M, Deriche R, Knösche TR, Anwander A (2009) Deterministic and probabilistic tractography based on complex fibre orientation distributions. *IEEE transactions on medical imaging*



28: 269–86.

3. Hagmann P, Cammoun L, Gigandet X, Meuli R, Honey CJ, et al. (2008) Mapping the structural core of human cerebral cortex. *PLoS biology* 6: 1479–1493.
4. Wedeen VJ, Wang RP, Schmahmann JD, Benner T, Tseng WYI, et al. (2008) Diffusion spectrum magnetic resonance imaging (DSI) tractography of crossing fibers. *NeuroImage* 41: 1267–77.
5. Wedeen VJ, Rosene DL, Wang R, Dai G, Mortazavi F, et al. (2012) The geometric structure of the brain fiber pathways. *Science (New York, NY)* 335: 1628–34.
6. Greenberg AS, Verstynen T, Chiu YC, Yantis S, Schneider W, et al. (2012) Visuotopic cortical connectivity underlying attention revealed with white-matter tractography. *The Journal of neuroscience : the official journal of the Society for Neuroscience* 32: 2773–82.
7. Verstynen T, Jarbo K, Pathak S, Schneider W (2011) In vivo mapping of microstructural somatotopies in the human corticospinal pathways. *Journal of neurophysiology* 105: 336–46.
8. Verstynen TD, Badre D, Jarbo K, Schneider W (2012) Microstructural organizational patterns in the human corticostriatal system. *Journal of neurophysiology* .
9. Makris N, Papadimitriou GM, Kaiser JR, Sorg S, Kennedy DN, et al. (2009) Delineation of the middle longitudinal fascicle in humans: a quantitative, in vivo, DT-MRI study. *Cerebral cortex (New York, NY : 1991)* 19: 777–85.
10. Wang Y, Fernández-Miranda JC, Verstynen T, Pathak S, Schneider W, et al. (2012) Rethinking the Role of the Middle Longitudinal Fascicle in Language and Auditory Pathways. *Cerebral Cortex* : 1–10.
11. Catani M, Dell’acqua F, Vergani F, Malik F, Hodge H, et al. (2012) Short frontal lobe connections of the human brain. *Cortex* 48: 273–91.
12. Catani M, Mesulam MM, Jakobsen E, Malik F, Matersteck a, et al. (2013) A novel frontal pathway underlies verbal fluency in primary progressive aphasia. *Brain* .
13. Jarbo K, Verstynen T, Schneider W (2012) In vivo quantification of global connectivity in the human corpus callosum. *NeuroImage* 59: 1988–1996.
14. Van Essen DC, Ugurbil K, Auerbach E, Barch D, Behrens TEJ, et al. (2012) The Human Connectome Project: a data acquisition perspective. *NeuroImage* 62: 2222–31.
15. Honey CJ, Sporns O, Cammoun L, Gigandet X, Thiran JP, et al. (2009) Predicting human resting-state functional connectivity from structural connectivity. *PNAS* 106: 2035–2040.
16. Pyles Ja, Verstynen TD, Schneider W, Tarr MJ (2013) Explicating the Face Perception Network with White Matter Connectivity. *PLoS ONE* 8: e61611.
17. Jbabdi S, Sotiropoulos SN, Behrens TE (2013) The topographic connectome. *Current Opinion in Neurobiology* : 1–9.
18. Moberts B, Vilanova A, Van Wijk JJ (2005) Evaluation of Fiber Clustering Methods for Diffusion Tensor Imaging. *IEEE Visualization* : 65–72.
19. O’Donnell LJ, Golby AJ, Westin CF (2013) Fiber clustering versus the parcellation-based connectome. *NeuroImage* .

20. Shimony JS, Snyder AZ, Lori N, Conturo TE (2002) Automated Fuzzy Clustering of Neuronal Pathways in Diffusion Tensor Tracking. Proceedings of the International Society of Magnetic Resonance Imaging in Medicine .
21. Li H, Xue Z, Guo L, Liu T, Hunter J, et al. (2010) A hybrid approach to automatic clustering of white matter fibers. *NeuroImage* 49: 1249–58.
22. O'Donnell L, Westin CF (2005) White matter tract clustering and correspondence in populations. Medical image computing and computer-assisted intervention : MICCAI International Conference on Medical Image Computing and Computer-Assisted Intervention 8: 140–7.
23. Jonasson L, Hagmann P, Thiran JP, Wedeen VJ (2005) Fiber tracts of high angular resolution diffusion MRI are easily segmented with spectral clustering. Proceedings of the International Society of Magnetic Resonance Imaging in Medicine .
24. Wassermann D, Descoteaux M, Deriche R (2008) Diffusion maps clustering for magnetic resonance q-ball imaging segmentation. *International Journal of Biomedical Imaging* .
25. Tsai A, Westin CF, Hero III AO, Willsky AS (2007) Fiber Tract Clustering on Manifolds With Dual Rooted-Graphs. In: IEEE Conference on Computer Vision and Pattern Recognition. Minneapolis, MN, pp. 1–6. doi:10.1109/CVPR.2007.383096.
26. Gerig G, Gouttard S, Corouge I (2004) Analysis of Brain White Matter via Fiber Tract Modeling. In: Proceedings of the 26th Annual International Conference of the IEEE EMBS. San Francisco, CA, USA, pp. 4421–4424.
27. Corouge I, Gouttard S, Gerig G (2004) Towards a Shape Model of White Matter Fiber Bundles Using Diffusion Tensor MRI. In: International Symposium on Biomedical Imaging (ISBI). pp. 344–347.
28. Prasad G, Joshi SH, Jahanshad N, Villalon J, Aganj I, et al. (2011) White Matter Tract Analysis in 454 Adults using Maximum Density Paths. MICCAI 2011 Workshop on Computational Diffusion MRI .
29. Xia Y, Turken U, Whitfield-Gabrieli SL, Gabrieli JD (2005) Knowledge-based classification of neuronal fibers in entire brain. Medical image computing and computer-assisted intervention : MICCAI International Conference on Medical Image Computing and Computer-Assisted Intervention 8: 205–12.
30. Ding Z, Gore JC, Anderson AW (2003) Classification and Quantification of Neuronal Fiber Pathways Using Diffusion Tensor MRI. *Magnetic Resonance in Medicine* 49: 716 –721.
31. Guevara P, Poupon C, Rivière D, Cointepas Y, Descoteaux M, et al. (2011) Robust clustering of massive tractography datasets. *NeuroImage* 54: 1975–1993.
32. Wassermann D, Bloy L, Kanterakis E, Verma R, Deriche R (2010) Unsupervised white matter fiber clustering and tract probability map generation: applications of a Gaussian process framework for white matter fibers. *NeuroImage* 51: 228–41.
33. Zhang S, Laidlaw DH (2005) DTI Fiber Clustering and Cross-subject Cluster Analysis. Proceedings of the International Society of Magnetic Resonance Imaging in Medicine : 2727.
34. Hartigan JA (1981) Consistency of Single Linkage for High-Density Clusters. *Journal of the American Statistical Association* 76: 388–394.

35. Wassermann D, Deriche R (2008) Simultaneous Manifold Learning and Clustering : Grouping White Matter Fiber Tracts Using a Volumetric White Matter Atlas. MICCAI 2008 Workshop - Manifolds in Medical Imaging: Metrics, Learning and Beyond2 : 1–8.
36. Zvitia O, Mayer A, Greenspan H (2008) Adaptive Mean-Shift Registration of White Matter Tractographies. 5th IEEE International Symposium on Biomedical Imaging : 692–695.
37. Brun A, Knutsson H, Park Hj, Shenton ME, Westin Cf (2004) Clustering Fiber Traces Using Normalized Cuts. In: Barillot C, Haynor DR, Hellier P, editors, Medical Image Computing and Computer-Assisted Intervention - MICCAI 2004. Springer-Verlag, pp. 368–375.
38. Wang X, Grimson WEL, Westin Cf (2011) Tractography segmentation using a hierarchical Dirichlet processes mixture model. *NeuroImage* 54: 290–302.
39. Hartigan J (1975) Clustering Algorithms. John Wiley & Sons.
40. Billingsley P (2012) Probability and Measure. Wiley.
41. Rao P (1983) Nonparametric Functional Estimation. Orlando, Florida: Academic Press.
42. Wishart D (1969) Mode analysis: a generalization of nearest neighbor which reduces chaining effects. In: Cole AJ, editor, Proceedings of the Colloquium on Numerical Taxonomy held in the University of St. Andrews. pp. 282–308.
43. Maier M, Hein M, von Luxburg U (2009) Optimal construction of k-nearest-neighbor graphs for identifying noisy clusters. *Theoretical Computer Science* 410: 1749–1764.
44. Chaudhuri K, Dasgupta S (2010) Rates of convergence for the cluster tree. In: Advances in Neural Information Processing Systems 23. Vancouver, BC, pp. 343–351.
45. Kpotufe S, Luxburg UV (2011) Pruning nearest neighbor cluster trees. *Proceedings of the 28th International Conference on Machine Learning* 105: 225–232.
46. Devroye LP, Wagner TJ, Devroye BYLP (1977) The Strong Uniform Consistency of Nearest Neighbor Density Estimates. *The Annals of Statistics* 5: 536–540.
47. Rinaldo A, Wasserman L (2010) Generalized density clustering. *The Annals of Statistics* 38: 2678–2722.
48. Rinaldo A, Singh A, Nugent R, Wasserman L (2012) Stability of Density-Based Clustering. *Journal of Machine Learning Research* 13: 905–948.
49. Ferraty F, Vieu P (2006) Nonparametric Functional Data Analysis. Springer.
50. Zhang S, Correia S, Laidlaw DH (2008) Identifying white-matter fiber bundles in DTI data using an automated proximity-based fiber-clustering method. *IEEE transactions on visualization and computer graphics* 14: 1044–53.
51. Garyfallidis E, Brett M, Amirbekian B, Nguyen C, Yeh Fc, et al. (2011) Dipy - a novel software library for diffusion MR and tractography. In: 17th Annual Meeting of the Organization for Human Brain Mapping. pp. 1–5.
52. Arthur D, Vassilvitskii S (2007) k-means ++ : The Advantages of Careful Seeding. In: ACM-SIAM Symposium on Discrete Algorithms. pp. 1027–1035. doi:10.1145/1283383.1283494.

53. Hastie T, Tibshirani R, Friedman J (2009) The Elements of Statistical Learning. Springer, second edition, 510–526 pp. doi:978-0387848570.
54. von Luxburg U (2006) A Tutorial on Spectral Clustering. Technical Report August, Max Planck Institute for Biological Cybernetics, Tuebingen.
55. Coifman RR, Lafon S (2006) Diffusion maps. *Applied and Computational Harmonic Analysis* 21: 5–30.
56. Ester M, Kriegel Hp, Xu X (1996) A Density-Based Algorithm for Discovering Clusters in Large Spatial Databases with Noise. In: *Knowledge Discovery and Data Mining*. pp. 226–231.
57. R Core Team (2012) R: A Language and Environment for Statistical Computing. Technical report, R Foundation for Statistical Computing, Vienna, Austria. doi:3-900051-07-0. URL <http://www.r-project.org/>.
58. Pedregosa F, Varoquaux G, Gramfort A, Michel V, Thirion B, et al. (2011) Scikit-learn : Machine Learning in Python. *Journal of Machine Learning Research* 12: 2825–2830.
59. Richards JW, Freeman PE, Lee AB, Schafer CM (2009) Exploiting Low-Dimensional Structure in Astronomical Spectra. *The Astrophysical Journal* 691: 32–42.
60. Richards JW, Freeman PE, Lee AB, Schafer CM (2009) Accurate parameter estimation for star formation history in galaxies using SDSS spectra. *Monthly Notices of the Royal Astronomical Society* 399: 1044–1057.
61. Yeh FC, Tseng WYI (2011) NTU-90: a high angular resolution brain atlas constructed by q-space diffeomorphic reconstruction. *NeuroImage* 58: 91–9.
62. Ashburner J, Friston KJ (1999) Nonlinear Spatial Normalization Using Basis Functions. *Human Brain Mapping* 7: 254–266.
63. Yeh FC, Wedeen VJ, Tseng WYI (2010) Generalized q-sampling imaging. *IEEE transactions on medical imaging* 29: 1626–35.
64. Bassar PJ, Pajevic S, Pierpaoli C, Duda J, Aldroubi a (2000) In vivo fiber tractography using DT-MRI data. *Magnetic resonance in medicine : official journal of the Society of Magnetic Resonance in Medicine / Society of Magnetic Resonance in Medicine* 44: 625–32.
65. Lazar M, Weinstein DM, Tsuruda JS, Hasan KM, Arfanakis K, et al. (2003) White matter tractography using diffusion tensor deflection. *Human brain mapping* 18: 306–21.
66. Haber SN, Knutson B (2010) The reward circuit: linking primate anatomy and human imaging. *Neuropsychopharmacology : official publication of the American College of Neuropsychopharmacology* 35: 4–26.
67. Azzalini A, Torelli N (2007) Clustering via nonparametric density estimation. *Statistics and Computing* 17: 71–80.
68. Draganski B, Kherif F, Klöppel S, Cook Pa, Alexander DC, et al. (2008) Evidence for segregated and integrative connectivity patterns in the human Basal Ganglia. *The Journal of neuroscience : the official journal of the Society for Neuroscience* 28: 7143–52.
69. Graybiel AM, Ragsdale CW (1978) Histochemically distinct compartments in the striatum of human, monkey, and cat demonstrated by acetylthiocholinesterase staining. *Proceedings of the National Academy of Sciences of the United States of America* 75: 5723–5726.

70. Ragsdale CW, Graybiel AM (1990) A simple ordering of neocortical areas established by the compartmental organization of their striatal projections. *Proceedings of the National Academy of Sciences of the United States of America* 87: 6196–9.
71. Ben-Hur A, Elisseeff A, Guyon I (2002) A stability based method for discovering structure in clustered data. In: *Pacific Symposium on Biocomputing*. volume 17, pp. 6–17.
72. Smith SP, Dubes R (1980) Stability of a hierarchical clustering. *Pattern Recognition* 12: 177–187.